SCIENCE CHINA
Technological Sciences

Special Issue: Celebrating the 100th Anniversary of Harbin Institute of Technology
•Article•

August 2020 Vol.63 No.8: 1426–1435
https://doi.org/10.1007/s11431-020-1670-4

High-content graphene nanoplatelet reinforced aluminum composites produced by ball milling and hot extrusion

ZHENG Zhong, ZHANG XueXi*, LI JianChao & GENG Lin

School of Materials Science and Engineering, Harbin Institute of Technology, Harbin 150001, China

Received March 11, 2020; accepted June 4, 2020; published online July 17, 2020

Due to the high specific surface area of graphene, the effective incorporation of high-content graphene in metals is challenging. Here, aluminum composites with graphene nanoplatelet (GNP) content up to 5.0 vol% were prepared by spark plasma sintering (SPS) of blended powders with various ball milling regimes and subsequent hot extrusion. The effects of GNP distribution state on the properties of GNP/Al composite were investigated. 5.0 vol% GNPs were uniformly dispersed in aluminum matrix by high-speed ball milling (HSBM) process, but with damage GNPs due to the too high energy input. By contrast, the well-structured and dispersed GNPs in aluminum powders were obtained via shift-speed ball milling (SSBM). The clear GNP-Al interface in extruded SSBM composite was attributed to well-structured GNPs. As a result, the yield strength (YS) and ultimate tensile strength (UTS) of composite produced by SSBM reached 279 and 303 MPa, which are 166% and 116% higher than those of monolithic Al. This demonstrated that it may be promising to introduce high-content GNPs with tailorable interface in Al alloys via modified ball milling technique and hot extrusion.

aluminum-matrix composites, graphene nanoplatelet, ball milling, hot extrusion, mechanical properties

Citation: Zheng Z, Zhang X X, Li J C, et al. High-content graphene nanoplatelet reinforced aluminum composites produced by ball milling and hot extrusion. Sci China Tech Sci, 2020, 63: 1426–1435, https://doi.org/10.1007/s11431-020-1670-4

1 Introduction

Graphene has high modulus (1020 GPa) and strength (130 GPa) [1–3]. In addition, graphene shows superior physical properties such as high thermal conductivity (5000 $W\ m^{-1}\ K^{-1}$) and charge-mobility (200000 $cm^2\ V^{-1}\ s^{-1}$) [4,5]. As a result, graphene has become high-performance fillers for metals, polymers and ceramics. Graphene nanoplatelet (GNP) is stacks of graphene sheets along *c*-axis [1] and has excellent mechanical properties similar to graphene monolayers and low cost.

Introducing GNP in metals, such as aluminum, may enhance their modulus, strength, wear resistance and lower their coefficient of thermal expansion. The challenge of preparing GNP reinforced aluminum-matrix composites (AMCs) is tailoring GNP distribution state. This is usually difficult since GNP has a giant specific surface area. Powder metallurgy (PM) has been widely used to disperse graphene in aluminum alloys [6–9]; but often introduced unexpected damage of graphene structure or even formed amorphous phase [7,9], which have a detrimental impact on the mechanical properties of graphene/Al composites [10,11]. The damage graphene during ball milling of graphene/Al powders may induce the interface reaction between graphene and aluminum [9,12], which is unfavorable for improving the mechanical properties of graphene/Al composites.

By using a modified PM route, Zhang et al. [13,14] developed nano-laminate 1.5 vol% GNP/Al composite. The laminated architecture effectively enhanced the modulus and ultimate tensile strength (UTS). Some well-studied graphene/Al composites prepared by PM technique are summarized in Table 1. Some studies showed that graphene was

*Corresponding author (email: xxzhang@hit.edu.cn)

Table 1 GNP/Al composites synthesized by PM (ball milling+sintering)

Year	Composite ingredients	Ball-to-powder ratio	Ball-milling speed (r min^{-1})	Time (h)	Interfacial reaction	Ref.
2014	1.3 vol% graphene[a)]/6061Al	2.6:1	–	1.5	Yes, Al_4C_3	[18]
2014	0.67 vol% graphene[b)]/(Al-3.9Cu-1.5Mg)	10:1	75	12	No	[16]
2014	1.3 vol% graphene[a)]/Al	5:1	–	5	Yes, Al_4C_3	[6]
2015	2.7 vol% graphene[b)]/Al	40:1	180	2	No	[7]
2015	0.7 vol% graphene[c)]/Al	15:1	200	1	No	[20]
2015	0.06 vol% graphene[a)]/Al	20:1	150	7.5	Yes, Al_4C_3	[21]
2015	0.7 vol% graphene[c)]/2024Al	15:1	100	3	No	[9]
2016	0.05 vol% graphene[c)]/2024Al	15:1	600	6	Yes, Al_4C_3	[22]
2016	1.3 vol% graphene[a)]/Al	15:1	500	6	Yes, Al_4C_3	[23]
2017	1.0 vol% graphene/6061Al	10:1	360	1.5	No	[15]
2017	1 vol% graphene[d)]/Al-5Mg	10:1	360	20	Yes, Al_4C_3	[17]
2017	1.3 vol% graphene[c)]/Al	10:1	350	4	–	[24]
2017	0.3 vol% graphene[b)]/Al	10:1	250	4	Yes, Al_4C_3	[25]
2018	2.7 vol% graphene[a)]/2219Al	4:1	200	6	No	[26]
2018	3 vol% graphene[a)]/Al	5:1	200	2	No	[27]
2018	0.7 vol% graphene[a)]/Al	–	100	1	No	[28]
2018	1.3 vol% graphene[a)]/2009Al	–	200	2	Yes, Al_4C_3	[29]
2018	0.26 vol% graphene[a)]/Al	5:1	300	4	No	[30]
2018	0.53 vol% graphene[a)]/Al	5:1	200	5	No	[19]
2019	0.67 vol% graphene[a)]/Al	20:1	180	–	No	[31]
2019	2.6 vol% graphene[a)]/1060Al	5:1	200	10	Yes, Al_4C_3	[32]
2020	1 vol% graphene[a)]/Al	5:1	500	5	–	[33]

a) GNP—graphene nanoplatelets; b) GNF—graphene nanoflakes; c) FLG—few-layered grapheme; d) GO—graphene oxide.

not damaged by short-time high-speed ball milling (HSBM, 360 r min^{-1} for 1.5 h) [15] or long-time low-speed ball milling (LSBM, 75 r min^{-1} for 12 h) [16]; but the low milling energy could not induce homogeneous distribution of graphene in Al matrix [17,34,35]. By contrast, long-time HSBM contributed to homogeneous graphene in Al matrix, however may result in the formation of amorphous GNPs [17]. The shift-speed ball milling (SSBM) process was applied to fabricate graphene nanosheet (GNS)/Al composite by Jiang et al. [36]. During SSBM process, Al powders were flattened into flakes in the stage of LSBM, and then the Al flakes were cold-welded into lamellar-structured particles by HSBM. The fractured graphene embedded in the cold-welded Al particles may be protected from direct damage [18]. The compromise of both dispersion and integrity of GNP during ball milling is necessary. Our recent work demonstrated that GNP mainly attached on the surface of Al particles sheared by steel balls during ball milling process (LSBM, 200 r min^{-1} for 5 h). Therefore, ball milled Al powders exhibited higher specific surface area, which results in the improvement of 1.0 vol% GNP distribution [19]. In ref. [36], an inflection point of LSBM time was also proposed, at which Al flakes had high enough surface area to accommodate the GNSs. However, the LSBM process was not successful for 5.0 vol% GNP/Al composite because of the limited increase in the specific surface area for the ball milled Al powders. Here, the coordination of dispersion and integrity of high-content GNP was achieved via a two-step ball milling process: first-step dispersion of GNP on the surface of Al flakes by LSBM, and second-step dispersion of GNP into Al particles by cold welding during short-time HSBM. Subsequently, the milled powders were sintered into billets, which were then hot-extruded into rods. An effective method for preparing high-content GNP/Al composite with enhanced mechanical properties was demonstrated.

2 Experimental section

The gas atomized pure Al powders (purity≥99.99%) with an average diameter of 10±2 μm were supplied by Tianjiu Changsha Technology Company, as illustrated in Figure 1(a) and (b). The as-received GNPs (purity≥99.9%), with an average thickness of 5–10 nm, were supplied by Jicang Nano Technology Company, as depicted in Figure 1(c) and (d). The pure Al powders were milled with as-received GNPs using a planetary ball mill in the stainless-steel jar. The ball milling processes were conducted with stearic acid as pro-

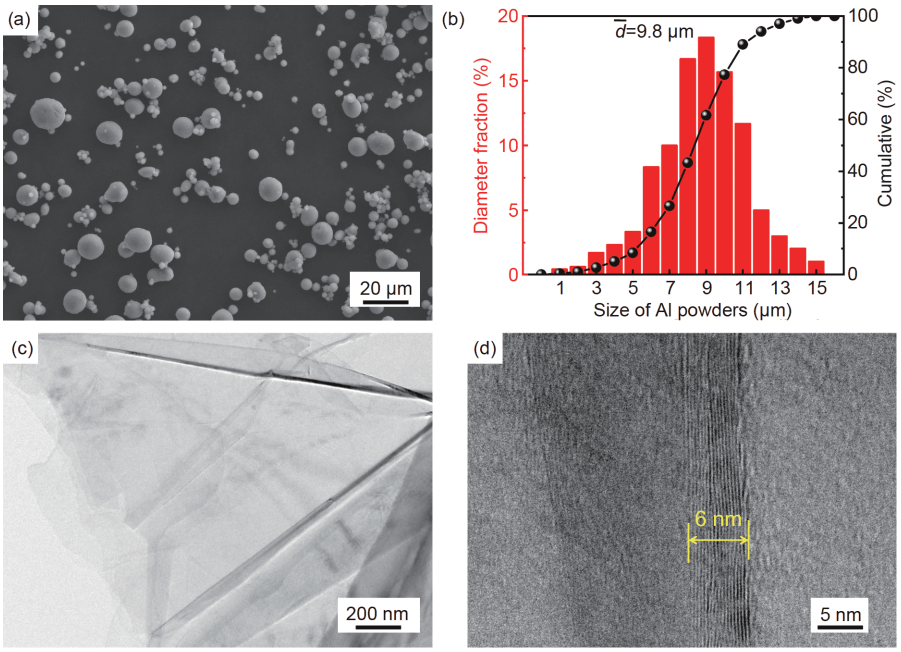

Figure 1 (Color online) (a) SEM image of the as-received Al powders; (b) statistical powder diameter distribution of the as-received Al powders; (c) TEM bright field image of as-received GNPs; (d) high resolution TEM (HRTEM) image of GNP.

cess control agent under argon atmosphere and a ball-to-powder ratio of 16:1. Three types of ball milling processes were conducted: (a) LSBM at a speed 100 r min^{-1} for 10 h; (b) HSBM at a speed of 300 r min^{-1} for 10 h; and (c) SSBM, that is LSBM at a speed of 100 r min^{-1} for 8 h followed by HSBM at a speed of 300 r min^{-1} for 2 h for a second time. The milled powders were sintered at a temperature of 550°C for 5 min under a uniaxial pressure of 50 MPa in vacuum in a HP-D250-1 spark plasma sintering (SPS) machine. The as-sintered ingots were heated at 450°C for 30 min and then extruded into rods with an extrusion ratio of 25:1. For comparison, monolithic Al samples were also prepared by the same routine.

The morphology of milled powders and microstructures of composites were observed by Zeiss field emission scanning electron microscope (SEM) Merlin Compact. Raman measurement was acquired using a Renishaw inVia Reflex Raman confocal microscope (Gloucestershire, UK) equipped with a diode laser emitting at 632.8 nm at a nominal power of 300 mW. Raman spectroscopy was employed to track the structural integrity of graphene in milled powders as a function of ball milling energy. The phases in as-sintered composites were characterized by Empyrean X-ray diffraction (XRD) with Cu-Kα radiation (λ=1.54 Å) in 2θ range of 20°–90° with a scan rate of 0.02° s^{-1} radiation. The samples for transmission electron microscope (TEM) analysis were prepared by ion thinning. A Talos F200X TEM was used to investigate the morphology of GNP, grains of aluminum matrix and interfacial reaction state. The mechanical properties of the monolithic Al and composite samples were characterized using dog-bone shaped samples on a universal testing machine Instron-5569. Tensile test was carried out at the room temperature with samples cut along the extrusion direction with a crosshead speed 0.5 mm min^{-1}. The dog-bone shaped samples had the gage length and diameter 25 and 5 mm, respectively. The elastic modulus (E) of monolithic Al and GNP/Al composite was measured by an Elastic Modulus and Damping System RFDA-HTVP1750C at room temperature. Rectangular bars with length 36 mm, thickness 4 mm and width 3 mm were prepared for E test.

3 Results and discussion

3.1 Microstructure of GNP/Al composites produced by various ball milling processes

Figure 2 shows the morphology of blended 5.0 vol% GNP/Al powders obtained by LSBM, SSBM and HSBM processes. Flat GNP/Al powder slices occurred after LSBM process (100 r min^{-1} for 10 h) (Figure 2(a)), while obvious cold-welding phenomenon happened after HSBM process (300 r min^{-1} for 10 h) (Figure 2(c)). By contrast, the SSBM process (100 r min^{-1} 8 h+300 r min^{-1} 2 h) produced blended GNP/Al powders as shown in Figure 2(b), e.g., slices and round-shaped cold-welded particles co-exist. The LSBM process produces irregular flakes while HSBM process creates spheroidal-like particles, while SSBM process lies in between. The thickness of Al flakes and particles was determined using 'Image pro plus', and their average thickness are shown in Figure 2(d). It can be seen that LSBM process

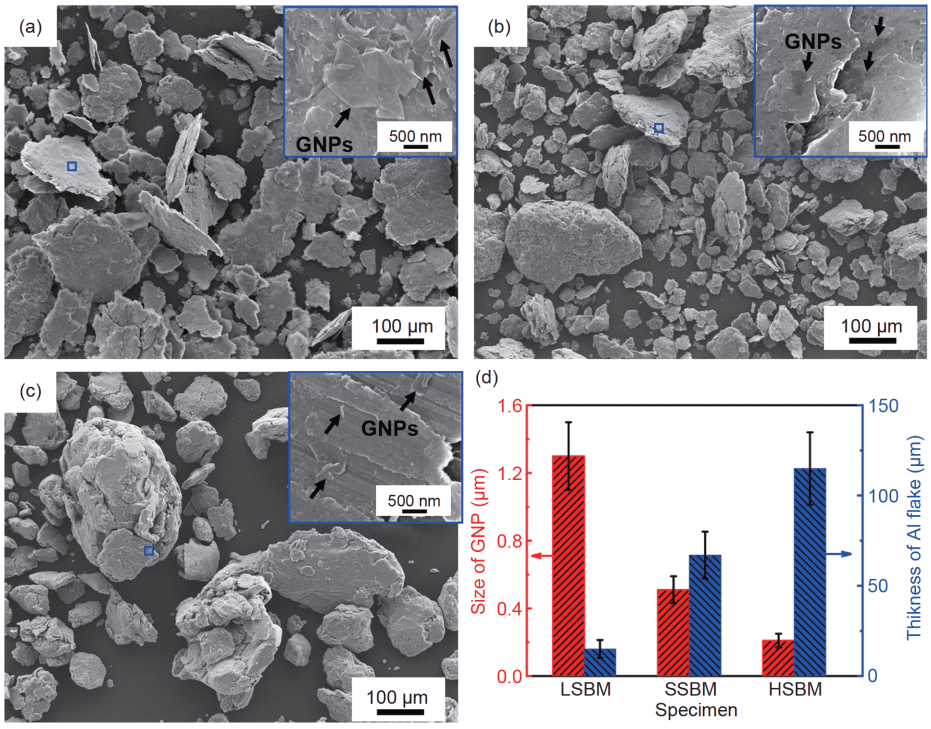

Figure 2 (Color online) SEM images showing morphology of blended GNP/Al powders. (a) LSBM GNP/Al powders; (b) SSBM GNP/Al powders; (c) HSBM GNP/Al powders; (d) statistical sizes of GNP and Al particle thickness. The insets in (a)–(c) show GNPs on the surface of Al particles.

produced thin Al flakes (~15 μm in thickness), while HSBM process produced large particles (~115 μm in thickness) due to cold welding. The average thickness of irregular shaped particles is about 67 μm for SSBM process.

On the other hand, multiple GNPs (insets in Figure 2(a)–(c)) on the surface of Al flakes and particles were counted from SEM images utilizing 'Image pro plus', and the average lateral sizes of GNPs are shown in Figure 2(d). The average lateral size of GNPs on the surface of Al flakes is about 1.3 μm in the inset of Figure 2(a), which is slightly smaller than that of as-received GNPs (lateral size ~1.5 μm). The GNP slices (~0.21 μm in lateral size) appeared on the surface of cold-welded Al particles using HSBM process (inset in Figure 2(c)). For SSBM processed powders, the GNPs show an average lateral size 0.51 μm (inset in Figure 2(b)).

The evolution of the sizes of Al particles and GNP flakes may be explained by the deformation of Al powders in various ball milling regimes: flattening of Al powders, cold-welding to produce cake- and spheroidal-like particles (Figure 3). The GNPs may be dispersed on irregular Al flakes by LSBM process as displayed in Figure 3(a). When Al powders are cold welded into spheroidal-like particles by HSBM process, the large GNP sheets break into smaller slices (Figure 3(b)) as a result of the forces generated between the powders and milling balls. For the SSBM process shown in Figure 3(c), the GNPs are pre-dispersed on the

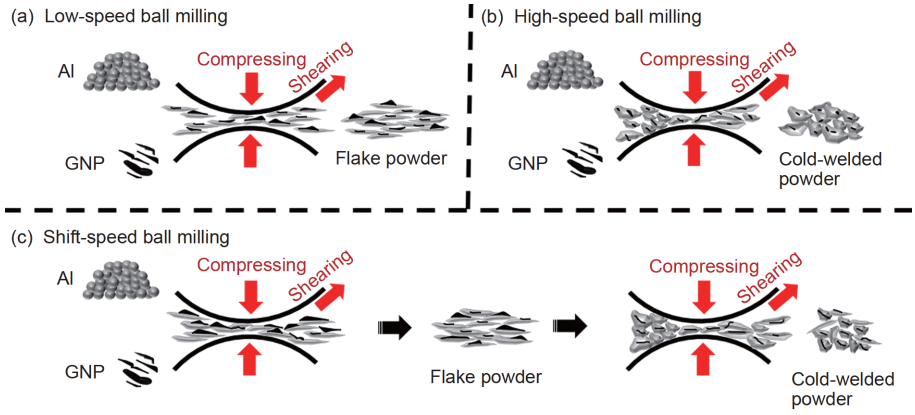

Figure 3 (Color online) The deformation of GNP/Al powders in various ball milling regimes. (a) LSBM process; (b) HSBM process; (c) SSBM process.

surface of Al flakes by LSBM. Then the blended GNP/Al powders are subjected to HSBM. The damage GNPs are reduced because GNPs are embedded into large Al particles via cold-welding during HSBM process.

The Raman spectrums of GNP/Al powders under different ball milling regimes are shown in Figure 4. One broad peak centered at 1343 cm^{-1} corresponding to the D band (disordered defect structure) and the other one centered at 1575 cm^{-1} to the G band (ordered graphene structure) [37]. The intensity ratio of D- to G-bands (I_D/I_G) represents defects and disorders in the graphene structure. The I_D/I_G value increases from 0.09 in the as-received GNPs to 1.46 in GNP/Al powders after HSBM process, implying the increase of the defect density in GNPs. It is noted that SSBM and LSBM processes have less impact on the I_D/I_G ratio (1.25 for SSBM, 1.23 for LSBM) than that of HSBM (1.46), which are acceptable in some studies prepared by ball milling [6,30,33,38]. Compared to the I_D/I_G value of 1.4 produced by low-energy ball milling (150 r min^{-1} for 1.5 h [33,38]), the achieved I_D/I_G by the present SSBM technique is much smaller, implying that embedding of GNPs in aluminum matrix effectively protect GNPs from serious damage.

It is well-known that graphene and Al are prone to react under high temperatures [9,12], especially at defect sites of graphene. In this work, we made use of SPS technique for the densification of blended GNP/Al powders and control the interfacial reaction between GNP and Al [27]. The XRD pattern of as-sintered composites under various ball milling regimes is displayed in Figure 5. It can be seen that a strong peak at 2θ=26.6° appears in the XRD pattern, corresponding to the presence of GNPs. At the same time, Al_4C_3 peaks exist for the composite produced via HSBM, but not for the SSBM and LSBM. The appearance of interfacial reaction between GNP and Al is thought to be related to the high I_D/I_G processed by HSBM for 10 h and thus the defects favor interfacial reaction. On the contrary, the absence of Al_4C_3 in composites after LSBM for 10 h and SSBM for 10 h reveals that the interfacial reaction may be too limited to be detectable via XRD.

Ball milling process can disperse the GNPs as well as reduce the grain size, which may remain in the composite after fast-speed SPS and extrusion. The microstructures of Al matrix, distribution of GNPs and GNP-Al interface are shown in Figure 6. Figure 6(a)–(c) shows the morphology of GNP in composites. In the HRTEM images (insets in Figure 6(a)–(c)), the lattice fringes have a spacing of 0.34 nm, which is the interplanar spacing of graphite (0002) [39]. GNP aggregates are observed in LSBM composite as indicated by blue dotted lines in Figure 6(a). On the other hand, dispersed GNPs exist at Al grain boundaries and in grains in SSBM and HSBM composites (Figure 6(b) and (c)), which is favorable for improving the mechanical properties of composites. In addition, damage of GNP due to

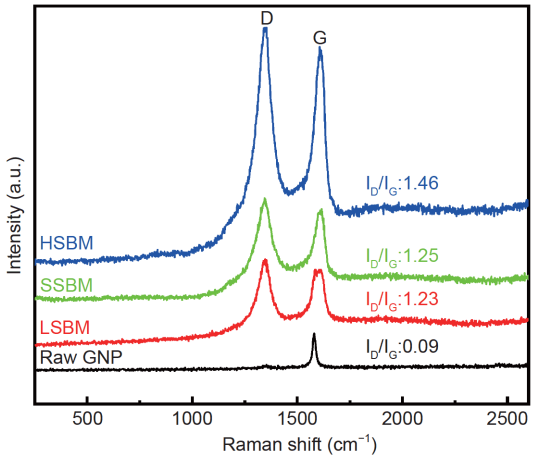

Figure 4 (Color online) Raman spectrums of raw GNPs and blended 5.0 vol% GNP/Al powders by LSBM process, SSBM process, and HSBM process.

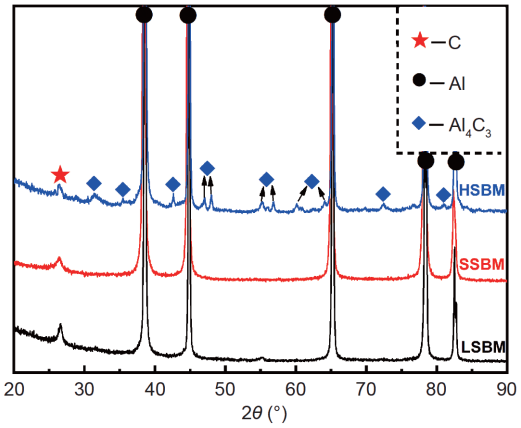

Figure 5 (Color online) XRD pattern of the 5.0 vol% GNP/Al composites densified by SPS. LSBM, SSBM and HSBM represent low-, shift- and high-speed ball milling process.

HSBM is also confirmed by HRTEM image in the inset of Figure 6(c), which should be owing to the high deformation energy input in HSBM process [36,40].

It is worth mentioning that an Al_4C_3 was observed in HSBM composite by the HRETEM image (inset in Figure 6(c)). The Al_4C_3 (0003) is confirmed by interplanar spacing of the lattice fringe 0.83 nm [6]. The HRTEM image also confirms the clean interface (no interfacial reaction) between well-structured GNP and Al in SSBM composite (inset in Figure 6(b)). In particular, the high-density dislocations and some stacking faults were produced inside Al grains in LSBM composite as shown in Figure 6(d) and its inset. Generally speaking, the high-density dislocations also can appear in Al grains owning to the higher deformation energy during SSBM and HSBM process, which are favorable for improving the composite strength.

The statistical grain sizes of monolithic Al and 5.0 vol% GNP/Al composite under various ball milling regimes were

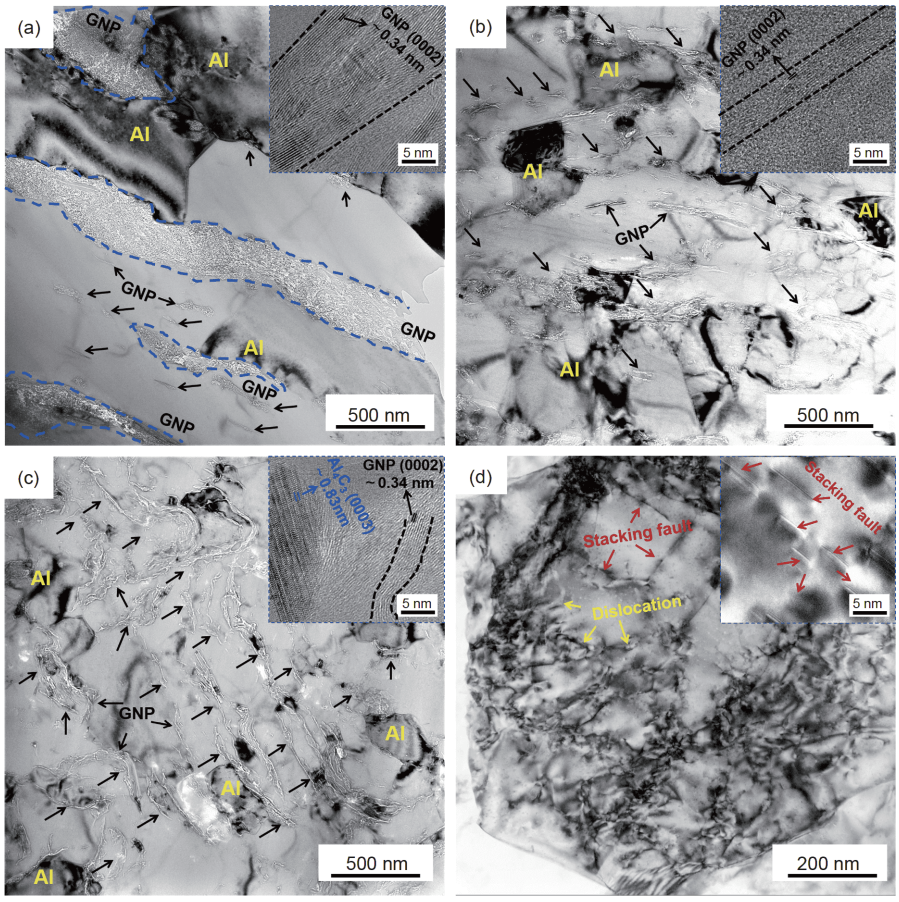

Figure 6 (Color online) Microstructure and distribution of GNPs in extruded 5.0 vol% GNP/Al composites. (a) LSBM process; (b) SSBM process; (c) HSBM process; (d) stacking fault and dislocations in Al grains of LSBM composite.

determined from TEM micrographs utilizing 'Image pro plus', and the average grain sizes are summarized in Table 2. Compared with the Al grain size in monolithic Al after LSBM for 10 h (~1.5 μm), the grain size in LSBM composite was reduced to 1.3 μm, implying that the addition of GNP is favorable for grain refinement. This is attributed to the presence of GNPs at Al grain boundaries, which reduced the mobility of the Al grain boundaries during high temperature dwelling and deformation processes. Furthermore, the grain sizes of composite and monolithic Al reduced with increasing ball milling energy.

3.2 Mechanical properties and strengthening mechanisms

The tensile stress-strain curves of monolithic Al and composite, processed by various ball milling methods, are shown in Figure 7. The *E*, yield strength (YS), UTS and fracture elongation are summarized in Table 3. It can be seen that the YS of HSBM Al (286 MPa) increases by 340% compared to that of LSBM Al (65 MPa), which may be ascribed to grain refinement and work-hardening strengthening [41]. On the other hand, the YS of HSBM composite (487 MPa) is 1.7

Table 2 The average grain size of monolithic Al and 5.0 vol% GNP/Al composite under various ball milling regimes

Materials	LSBM	SSBM	HSBM
Monolithic Al	1504±150 nm	941±130 nm	297±75 nm
Composite	1296±145 nm	720±129 nm	185±76 nm

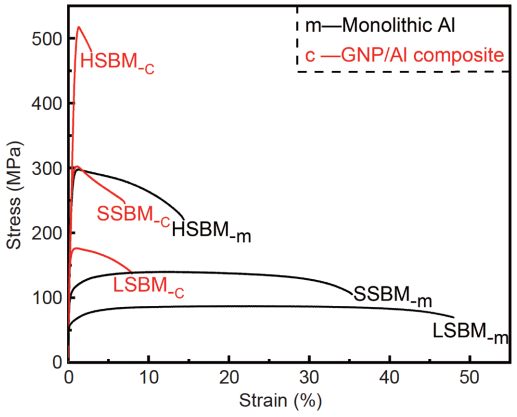

Figure 7 (Color online) Tensile stress-strain curves of extruded Al and GNP/Al composites processed by LSBM, SSBM and HSBM.

Table 3 The *E*, YS, UTS and fracture elongation of extruded Al and GNP/Al composites processed by LSBM, SSBM and HSBM

Specimen	*E* (GPa)	YS (MPa)	UTS (MPa)	Elongation (%)
LSBM-c	78.1±1.8	158±2	162±3	7.9±1.5
LSBM-m	71.1±2.1	65±2	86±2	48.0±5
SSBM-c	81.3±1.9	279±4	303±6	7.0±1.8
SSBM-m	71.0±1.7	105±2	140±3	35.3±6
HSBM-c	78.8±1.9	487±8	517±11	2.9±0.5
HSBM-m	73.0±2.5	286±5	297±9	14.5±4

times larger than that of Al (286 MPa), which is the outcome of well-dispersed GNPs and nano-grains in aluminum matrix (Figures 2 and 6). In particular, the ultra-high UTS of HSBM composite reaches 517 MPa. The UTS and YS of SSBM composite are 303 and 279 MPa, 116% and 166% higher than those of the SSBM Al, respectively. The tensile stress-strain curves contain unusual plastic and necking stages, i.e., necking started immediately after the occurrence of yielding phenomenon (Figure 7). It is generally considered that multiplication of grain boundaries by grain refinement makes dislocation movement more difficult and reduces the work hardening capacity [41]. At the same time, it is noticed that the UTS of Al and composite is linked inversely to their fracture elongation with increasing ball milling energy (LSBM → SSBM → HSBM). As shown in Table 3, the elongation of HSBM composite is <3% because of the high-density dislocation and introduction of Al_4C_3 [19]. While the 0.5 vol% GNS/Al composite produced via SSBM (6 h LSBM plus 0.5 h HSBM) exhibited a better balance between tensile strength (295 MPa) and ductility (13.5%) [36]. Generally, the synergistic effects of ultrafine-grained Al matrices and uniformly dispersed GNSs are considered responsible for such exceptional properties. Furthermore, the *E* of SSBM composite is 14.5% higher than that of Al. The much-enhanced *E* can also be attributed to the homogeneously distributed high-content GNPs.

Figure 8 shows the fracture surfaces of composites processed by LSBM, SSBM and HSBM. It can be seen that dimples exist on the fracture surface of all composites. Multiple GNPs can be observed on the fracture surface of LSBM composite, as depicted in Figure 8(a). On the other hand, thin GNP slices and Al_4C_3 rods appear on the fracture surface of HSBM composite (Figure 8(c)). The fracture morphology implies that GNP aggregates still exist in LSBM composite, while GNPs were effectively dispersed in SSBM and HSBM composites. As a result, in SSBM and HSBM composites, the homogeneously distributed GNPs may act as effective reinforcements for enhancing mechanical properties of composites.

The fracture behaviors of LSBM, SSBM and HSBM composites are schematically shown in Figure 9. Because GNP aggregates existed in LSBM composite, the fractures are considered to be caused by de-bonding and pull-out of GNP from Al matrix (Figure 9(a)). With increasing ball milling energy, GNPs disperse in Al matrix and act as reinforcements by bridging the cracks, leading to exposure of many GNP slices on the fracture surfaces, as shown in Figure 9(b) and (c). The dispersed GNPs exhibit significant load transfer strengthening effect and thus improve the mechanical properties of composites. It is worth mentioning that the *in-situ* synthesized Al_4C_3 rods, together with dispersed GNPs may have obvious load transfer strengthening in HSBM composite. In this work, GNPs are dispersed homogeneously via SSBM and HSBM processes, which are generally satisfied with this model.

From Figure 7, it is noticed that the UTS of composite is linked inversely to the fracture strain, which is the usual cases for graphene/Al composites [7,8,10–14,20,25,28,31,42–46]. Some graphene/Al composites can simultaneously achieve super-high strength and toughness [8,10,13,47]. In this work, the mechanical properties of extruded SSBM composite had a UTS 303 MPa and elongation 7.0%, im-

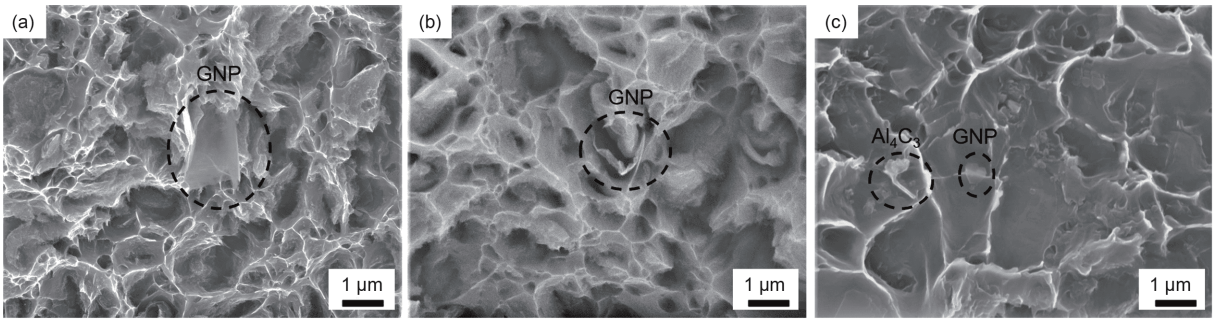

Figure 8 SEM images showing the fracture surfaces of GNP/Al composites. (a) LSBM; (b) SSBM; (c) HSBM.

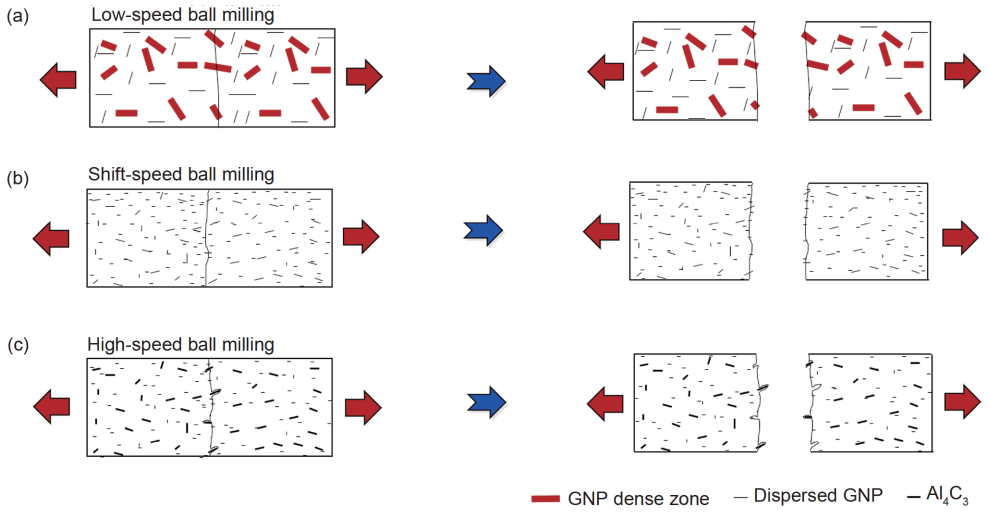

Figure 9 (Color online) The fracture behaviors of GNP/Al composites with various distribution states of GNP. (a) The presence of GNP aggregates after LSBM; (b), (c) homogeneous distribution of GNPs produced by SSBM and HSBM processes.

plying that the present SSBM technique effectively dispersed GNPs in Al matrix without excessive damage GNPs and formation of unfavorable amorphous phase [48–50]. The UTS and elongation of the present work and some well-studied GNPs reinforced pure Al composites are shown in Figure 10(a). It can be seen that the UTS shows strong dependence on preparation techniques. The composites with homogeneous distribution of graphene via secondary-processing, including rolling and extrusion, usually exhibited higher UTS than those of the hot press sintered composites.

It should be noted that the contents of graphene are different in these work. A normalized parameter $R=(\sigma_c-\sigma_m)/V_r\sigma_m$, where σ_c and σ_m are UTS of composite and monolithic Al respectively, and V_r is the volume fraction of GNP, was defined to reflect the strengthening efficiency of the reinforcement [19]. The results of this work and some other well-studied composites are shown in Figure 10(b). Here, the different R value should be attributed to the difference in graphene/Al interfacial reaction, graphene dispersion state and their sizes. Usually, graphene/Al composites showed low R value owning to graphene aggregation [35] or serious interfacial reaction [11]. In graphene/Al composites, the larger-sized graphene contributed a lot to the load transfer, while the smaller ones contributed more to the Orowan strengthening [47]. So, the improved strengthening efficiency for graphene in composite can be obtained by controlling graphene size. Our previous work showed that graphene/Al composites prepared by multiple cold-drawing had a high R due to the well interfacial bonding states [19]. In this study, the combination SSBM and hot extrusion processes significantly improved the distribution of well-structured GNPs, as demonstrated in Figures 2 and 6. However, the R of GNP was not that high (Figure 10(b)) although an ultra-high UTS in SSBM composite was obtained. The thickness of GNPs was still large in GNP/Al composite (the insets in Figure 6(a)–(c)), but their lateral size was reduced (Figure 2(d)). The GNP/Al composites under various ball milling regimes showed the similar strengthening efficiency of GNP.

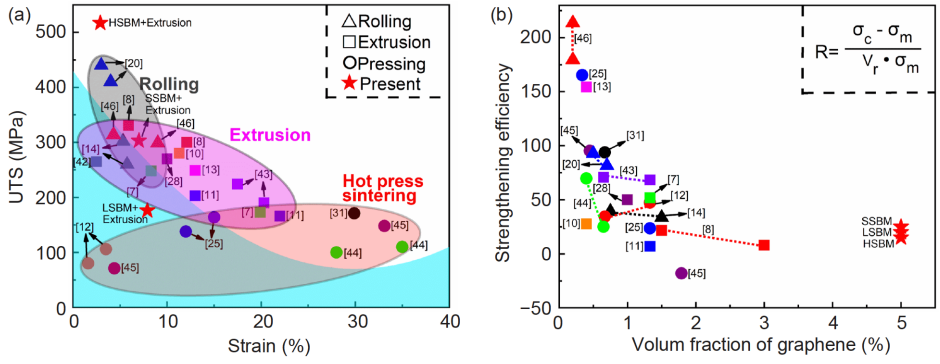

Figure 10 (Color online) Mechanical properties of graphene reinforced Al composites produced by various techniques. (a) UTS vs. fracture elongation in the present work (ball milling+extrusion) and composites including hot press sintering [12,25,31,44,45], extrusion [7,8,10,11,13,28,42,43] and rolling [14,20,46]. (b) Strengthening efficiency (R) vs. volume fraction of graphene in the current research and some well-studied composites [13,25,31,45,46].

The result showed that getting enhanced R of GNP in the present 5.0 vol% GNP/Al composite should reduce the GNP thickness in order to improve the homogeneous distribution state without damage GNPs [51].

4 Conclusions

The 5.0 vol% GNP/Al powders were prepared by various ball milling processes including HEBM, SSBM and LSBM. The GNP/Al composites were fabricated by SPS and subsequent hot extrusion. The microstructures and mechanical properties were investigated in relation to various ball milling regimes. The main conclusions can be drawn as follows.

(1) SSBM induced homogeneous dispersion of high-content GNPs in aluminum matrix while kept well-structured GNPs. The LSBM stage pre-dispersed GNPs on the surface of Al flakes while the HSBM stage caused entrapment of GNPs in large particles via cold-welding process.

(2) Interfacial reaction between GNP and Al occurred in the HSBM composite, but was absent in SSBM and LSBM composites. The absence of Al_4C_3 in SSBM and LSBM composites was related to the limited energy input during ball milling and well-structured GNP.

(3) The dispersed GNPs with well-structure existed at Al grain boundaries and in grains in SSBM composite. The extruded SSBM composite had UTS 303 MPa and elongation 7.0%. The improved UTS of SSBM composite was attributed to the homogeneous dispersion of GNPs, grain refinement and high-density dislocations.

This work was supported by the National Key R&D Program of China (Grant No. 2017YFB0703103), and Guangdong Province Key Area R&D Program (Grant No. 2019B010942001).

1 Dorri Moghadam A, Omrani E, Menezes P L, et al. Mechanical and tribological properties of self-lubricating metal matrix nanocomposites reinforced by carbon nanotubes (CNTs) and grapheme: A review. Compos Part B-Eng, 2015, 77: 402–420
2 Tsai J L, Tu J F. Characterizing mechanical properties of graphite using molecular dynamics simulation. Mater Des, 2010, 31: 194–199
3 King A, Johnson G, Engelberg D, et al. Observations of intergranular stress corrosion cracking in a grain-mapped polycrystal. Science, 2008, 321: 382–385
4 Balandin A A, Ghosh S, Bao W, et al. Superior thermal conductivity of single-layer graphene. Nano Lett, 2008, 8: 902–907
5 Bolotin K I, Sikes K J, Jiang Z, et al. Ultrahigh electron mobility in suspended graphene. Solid State Commun, 2008, 146: 351–355
6 Pérez-Bustamante R, Bolaños-Morales D, Bonilla-Martínez J, et al. Microstructural and hardness behavior of graphene-nanoplatelets/aluminum composites synthesized by mechanical alloying. J Alloys Compd, 2014, 615: S578–S582
7 Li J L, Xiong Y C, Wang X D, et al. Microstructure and tensile properties of bulk nanostructured aluminum/graphene composites prepared via cryomilling. Mater Sci Eng-A, 2015, 626: 400–405
8 Li Z, Fan G, Guo Q, et al. Synergistic strengthening effect of graphene-carbon nanotube hybrid structure in aluminum matrix composites. Carbon, 2015, 95: 419–427
9 Shin S E, Bae D H. Deformation behavior of aluminum alloy matrix composites reinforced with few-layer graphene. Compos Part A-Appl Sci Manu, 2015, 78: 42–47
10 Rashad M, Pan F, Tang A, et al. Effect of Graphene nanoplatelets addition on mechanical properties of pure aluminum using a semi-powder method. Prog Nat Sci-Mater Int, 2014, 24: 101–108
11 Rashad M, Pan F, Yu Z, et al. Investigation on microstructural, mechanical and electrochemical properties of aluminum composites reinforced with graphene nanoplatelets. Prog Nat Sci-Mater Int, 2015, 25: 460–470
12 Bisht A, Srivastava M, Kumar R M, et al. Strengthening mechanism in graphene nanoplatelets reinforced aluminum composite fabricated through spark plasma sintering. Mater Sci Eng-A, 2017, 695: 20–28
13 Wang J, Li Z, Fan G, et al. Reinforcement with graphene nanosheets in aluminum matrix composites. Scripta Mater, 2012, 66: 594–597
14 Li Z, Guo Q, Li Z, et al. Enhanced mechanical properties of graphene (reduced graphene oxide)/aluminum composites with a bioinspired nanolaminated structure. Nano Lett, 2015, 15: 8077–8083
15 Liu G, Zhao N, Shi C, et al. *In-situ* synthesis of graphene decorated with nickel nanoparticles for fabricating reinforced 6061Al matrix composites. Mater Sci Eng-A, 2017, 699: 185–193
16 Yan S J, Dai S L, Zhang X Y, et al. Investigating aluminum alloy reinforced by graphene nanoflakes. Mater Sci Eng-A, 2014, 612: 440–444
17 Kwon H, Mondal J, AlOgab K A, et al. Graphene oxide-reinforced aluminum alloy matrix composite materials fabricated by powder metallurgy. J Alloys Compd, 2017, 698: 807–813
18 Bastwros M, Kim G Y, Zhu C, et al. Effect of ball milling on graphene reinforced Al6061 composite fabricated by semi-solid sintering. Compos Part B-Eng, 2014, 60: 111–118
19 Li J, Zhang X, Geng L. Improving graphene distribution and mechanical properties of GNP/Al composites by cold drawing. Mater Des, 2018, 144: 159–168
20 Shin S E, Choi H J, Shin J H, et al. Strengthening behavior of few-layered graphene/aluminum composites. Carbon, 2015, 82: 143–151
21 Czeppe T, Korznikova E, Ozga P, et al. Application of the high pressure torsion supported by mechanical alloying for the metal-graphene composites preparation. Mechanik, 2015, 147: 41–46
22 Shin S E, Ko Y J, Bae D H. Mechanical and thermal properties of nanocarbon-reinforced aluminum matrix composites at elevated temperatures. Compos Part B-Eng, 2016, 106: 66–73
23 Tabandeh-Khorshid M, Omrani E, Menezes P L, et al. Tribological performance of self-lubricating aluminum matrix nanocomposites: Role of graphene nanoplatelets. Eng Sci Tech Int J, 2016, 19: 463–469
24 Asgharzadeh H, Sedigh M. Synthesis and mechanical properties of Al matrix composites reinforced with few-layer graphene and graphene oxide. J Alloys Compd, 2017, 728: 47–62
25 Li G, Xiong B. Effects of graphene content on microstructures and tensile property of graphene-nanosheets/aluminum composites. J Alloys Compd, 2017, 697: 31–36
26 Pillari L K, Shukla A K, Murty S V S N, et al. On the comparison of graphene and multi-wall carbon nanotubes as reinforcements in aluminum alloy AA2219 processed by ball milling and spark plasma sintering. Trans Ind Inst Met, 2018, 71: 1099–1112
27 Hu Z, Chen F, Xu J, et al. 3D printing graphene-aluminum nanocomposites. J Alloys Compd, 2018, 746: 269–276
28 Yang W, Zhao Q, Xin L, et al. Microstructure and mechanical properties of graphene nanoplates reinforced pure Al matrix composites prepared by pressure infiltration method. J Alloys Compd, 2018, 732: 748–758
29 Zhang Z W, Liu Z Y, Xiao B L, et al. High efficiency dispersal and strengthening of graphene reinforced aluminum alloy composites fabricated by powder metallurgy combined with friction stir processing. Carbon, 2018, 135: 215–223
30 Li M, Gao H, Liang J, et al. Microstructure evolution and properties of graphene nanoplatelets reinforced aluminum matrix composites. Mater Charact, 2018, 140: 172–178
31 Bhadauria A, Singh L K, Laha T. Combined strengthening effect of

nanocrystalline matrix and graphene nanoplatelet reinforcement on the mechanical properties of spark plasma sintered aluminum based nanocomposites. Mater Sci Eng-A, 2019, 749: 14–26
32 Li J, Zhang X, Geng L. Effect of heat treatment on interfacial bonding and strengthening efficiency of graphene in GNP/Al composites. Compos Part A-Appl Sci Manu, 2019, 121: 487–498
33 Li M, Zhang Z, Gao H, et al. Formation of multilayer interfaces and the load transfer in graphene nanoplatelets reinforced Al matrix composites. Mater Charact, 2020, 159: 110018
34 Zhan K, Wu Y, Li J, et al. Investigation on surface layer characteristics of shot peened graphene reinforced Al composite by X-ray diffraction method. Appl Surf Sci, 2018, 435: 1257–1264
35 Latief F H, Sherif E S M. Effects of sintering temperature and graphite addition on the mechanical properties of aluminum. J Ind Eng Chem, 2012, 18: 2129–2134
36 Jiang Y, Tan Z, Xu R, et al. Tailoring the structure and mechanical properties of graphene nanosheet/aluminum composites by flake powder metallurgy via shift-speed ball milling. Compos Part A-Appl Sci Manu, 2018, 111: 73–82
37 Huang C, Hu S, Chen K. Influence of rolling temperature on the interfaces and mechanical performance of graphene-reinforced aluminum-matrix composites. Int J Miner Metall Mater, 2019, 26: 752–759
38 Ferrari A C, Robertson J. Interpretation of Raman spectra of disordered and amorphous carbon. Phys Rev B, 2000, 61: 14095–14107
39 Jiang L, Li Z, Fan G, et al. The use of flake powder metallurgy to produce carbon nanotube (CNT)/aluminum composites with a homogenous CNT distribution. Carbon, 2012, 50: 1993–1998
40 Yan L, Tan Z, Ji G, et al. A quantitative method to characterize the Al_4C_3-formed interfacial reaction: The case study of MWCNT/Al composites. Mater Charact, 2016, 112: 213–218
41 Howeyze M, Arabi H, Eivani A R, et al. Strengthening of AA5052 aluminum alloy by equal channel angular pressing followed by softening at room temperature. Mater Sci Eng-A, 2018, 720: 160–168
42 Bartolucci S F, Paras J, Rafiee M A, et al. Graphene-aluminum nanocomposites. Mater Sci Eng-A, 2011, 528: 7933–7937
43 Wang J, Zhang X, Zhao N, et al. *In situ* synthesis of copper-modified graphene-reinforced aluminum nanocomposites with balanced strength and ductility. J Mater Sci, 2019, 54: 5498–5512
44 Gao X, Yue H, Guo E, et al. Preparation and tensile properties of homogeneously dispersed graphene reinforced aluminum matrix composites. Mater Des, 2016, 94: 54–60
45 Bhadauria A, Singh L K, Laha T. Effect of physio-chemically functionalized graphene nanoplatelet reinforcement on tensile properties of aluminum nanocomposite synthesized via spark plasma sintering. J Alloys Compd, 2018, 748: 783–793
46 Zhao M, Xiong D B, Tan Z, et al. Lateral size effect of graphene on mechanical properties of aluminum matrix nanolaminated composites. Scripta Mater, 2017, 139: 44–48
47 Han T, Li J, Zhao N, et al. Microstructure and properties of copper coated graphene nanoplates reinforced Al matrix composites developed by low temperature ball milling. Carbon, 2020, 159: 311–323
48 Yue H, Yao L, Gao X, et al. Effect of ball-milling and graphene contents on the mechanical properties and fracture mechanisms of graphene nanosheets reinforced copper matrix composites. J Alloys Compd, 2017, 691: 755–762
49 Fu J, Wei C, Wang W, et al. Studies of structure and properties of graphene oxide prepared by ball milling. Mater Res Innova, 2015, 19: S1–S277
50 Rashad M, Pan F, Zhang J, et al. Use of high energy ball milling to study the role of graphene nanoplatelets and carbon nanotubes reinforced magnesium alloy. J Alloys Compd, 2015, 646: 223–232
51 Fadavi Boostani A, Yazdani S, Taherzadeh Mousavian R, et al. Strengthening mechanisms of graphene sheets in aluminium matrix nanocomposites. Mater Des, 2015, 88: 983–989